In situ Neutron Diffraction Studies of Carbide-Matrix Interactions in HAYNES® 230® Nickel Based Superalloy

Tarik A. Saleh[1,2], Bjørn Clausen[2], Donald W. Brown[2], Hahn Choo[1,3], Peter K. Liaw[1], Mark A. M. Bourke[2], Sven C. Vogel[2], Raymond A. Buchanan[1] and Dwaine L. Klarstrom[4]

1. Department of Materials Science and Engineering, University of Tennessee, Knoxville, TN 37996, U.S.A.
2. Los Alamos Neutron Science Center, Los Alamos National Laboratory, Los Alamos, NM 87545, U.S.A.
3. Metals and Ceramics Division, Oak Ridge National Laboratory, Oak Ridge, TN 37831, U.S.A.
4. Haynes International, Inc., Kokomo, IN 46904, U.S.A.

ABSTRACT

HAYNES 230 is a solid solution strengthened, face centered cubic (FCC), nickel-based superalloy, with a small amount (1-5 vol. %) of semi-coherent FCC carbides. Neutron diffraction experiments were performed to study the interaction of the carbides with the matrix during tensile and compressive loading. The behavior of the elastic lattice strains during *in situ* loading clearly showed a tension-compression asymmetry. Although the volume percentage is small, the interaction between the carbides and the matrix had a significant effect on the load sharing. In compression, the carbides began load sharing at the macroscopic yield point, while the tension test suggests no load sharing. Debonding at the carbide-matrix interface is proposed to explain the lack of load sharing during the tensile loading based on the disparities observed between the experimental results and the finite element models.

INTRODUCTION

HAYNES 230 alloy is a nickel-based solid-solution strengthened superalloy with a composition of 22Cr, 14W, 2Mo, 0.5Mn, 0.4Si, 0.3Al, 0.1C, 0.02 La, 5Co max, 3Fe max, 0.015B max, balance Ni in weight percent. There are 1-5 volume percent M_6C type carbides in the as-received condition. As the carbides provide a composite effect during loading, for clarity, the main crystalline structure of HAYNES 230 alloy will be referred to as the matrix.

The alloy is rolled from an electro-slag remelted slab ingot on a reversing mill at approximately 1200 °C. After rolling to the final gauge, the plate is solution annealed at 1200 °C and water quenched. Typical tensile properties of the alloy at ambient temperature are: 0.2% yield strength of 375 MPa, ultimate tensile strength of 844 MPa, and elongation at failure of 48% [1]. HAYNES 230 alloy is frequently used in fatigue intensive applications, such as power generation turbines. Its composition is optimized for use in high-temperature, oxidizing, and nitriding environments.

Neutron diffraction provides a nondestructive technique to evaluate the intergranular strain development due to mechanical loading in a material [2]. Coupling

neutron diffraction with a hydraulic mechanical testing machine, as at the Spectrometer for Materials Research at Temperature and Stress (SMARTS) at the Los Alamos Neutron Science Center (LANSCE) [3], allows intergranular strains to be monitored during uniaxial or fatigue loading. The geometry of SMARTS allows one to monitor the average strain in grains oriented with their plane normal parallel and perpendicular to the loading direction. These strains are referred to as the axial and transverse directions, respectively. This method can be applied to any polycrystalline material including metals, ceramics, and composites [4,5].

The present studies involved *in situ* tension and compression studies. These experiments provide a baseline measurement for future fatigue experiments, detailing the behavior of the alloy in a single cycle of fatigue. The carbides present in the alloy not only affected the loading behavior, but they produced a tension-compression asymmetry which motivated this study of the carbide-matrix interaction in this material.

EXPERIMENTAL DETAILS

Cylindrical tensile specimens were cut from 13mm thick plate, with a gauge-length of 50 mm and a diameter of 6 mm. The specimens had a surface roughness of 0.2 μm along the gauge-length section. The ends of the specimens were threaded with a ½" UNC 13 thread [6]. Compression specimens were cylinders of 20 mm in length and 10 mm in diameter.

The diffraction patterns were analyzed using the General Structure Analysis System (GSAS) software [7]. Both single peak fitting and Rietveld refinement were performed to yield the *hkl*-specific and lattice-parameter strains, respectively [2]. All strains reported below are relative to the starting condition of each sample under a nominal holding stress of 20 MPa in tension and -10 MPa in compression. A typical diffraction pattern is shown in Figure 1 with the main matrix peaks indexed, and the 333 carbide reflection noted as well. The carbide peak was only resolvable in the transverse diffraction bank, due to being overwhelmed by background scattering in the axial direction. The experimental

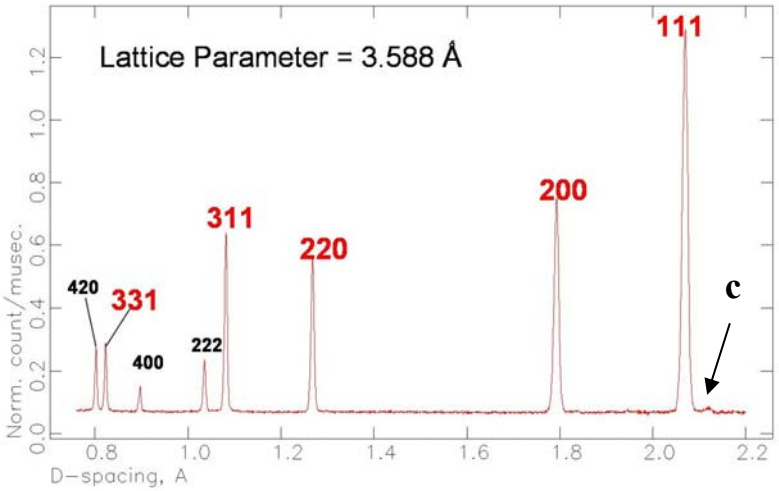

Figure 1: Diffraction pattern of HAYNES 230 with the peaks indexed. Lattice parameter derived from Rietveld refinement. 333 carbide peak indicated with "c".

carbide data presented is specific to this reflection and is not based on Rietveld-generated lattice-parameter strain.

In tension, the specimen was loaded incrementally from 20 MPa to 700 MPa and then unloaded to 20 MPa. The loading was paused for 10-15 minutes after each stress increment to collect diffraction patterns. Measurements were made at twenty-two stresses during loading and three during unloading (Figure 2a). Similarly, in compression, a sample was loaded from 10 MPa to 605 MPa, pausing for diffraction patterns at thirty-nine stresses during loading and four during unloading (Figure 2a).

MODELING

Finite element modeling (FEM) was performed using ABAQUS^{TM} software [8]. The carbide particles were modeled as cubes embedded in a matrix. This model has previously been successful in capturing the behavior of the elastic lattice-parameter strains in particle-strengthened composites [9]. The matrix properties were estimated from the bulk properties of the alloy, while the carbide's properties were estimated from similar carbides (Table 1). The matrix was modeled with an elastic-hardening bilinear curve, while the carbide was assumed to behave elastically. Each model used the experimental load levels as the applied load. The average of the FEM strains in each element at each load point in the loading axis (3 direction) is analogous to the experimental lattice parameter strains measured in the axial direction during loading. The average of the FEM strains in both the 1 and 2 directions for each element is analogous to the transverse lattice-parameter strains measured from the *in situ* neutron experiments. Residual strains present in HAYNES 230 in the as-received state were modeled by starting the simulation at a temperature of 600 ºC and cooling it to room

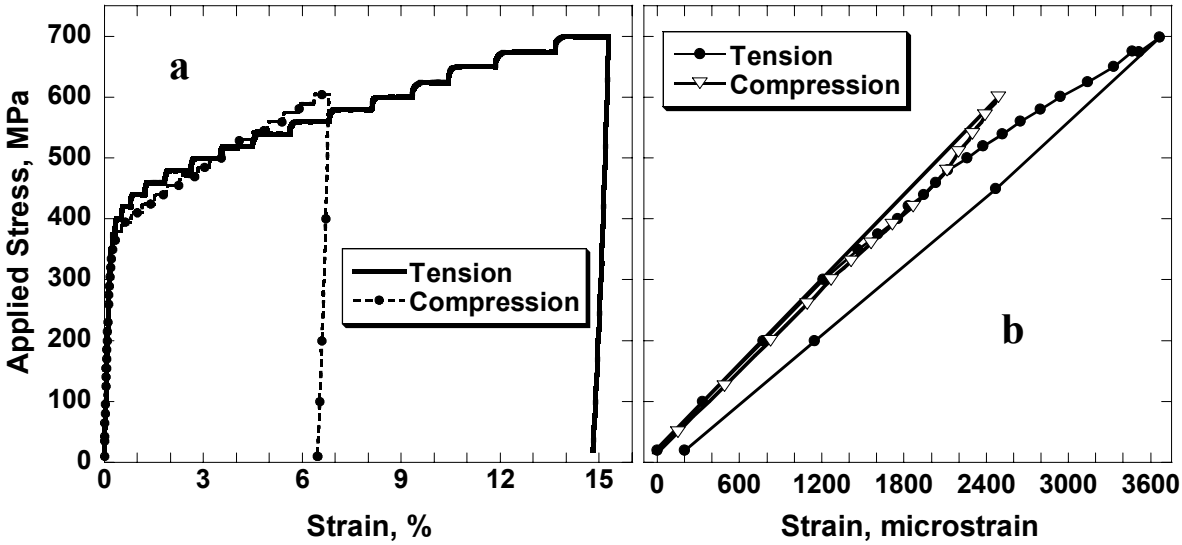

Figure 2: Tension-compression asymmetry in (a) the macroscopic stress-strain behavior and (b) the elastic lattice parameter strains in the axial direction.

temperature before load was applied. This mimics the thermal residual strains present due to differences in thermal expansion between the carbide and the matrix.

Table 1: Materials properties used in the FEM.

	Elastic Modulus (GPa)	Yield Strength (MPa)	Stress at ε = 47% (MPa)	Thermal Expansion (mm/mm/ºC)
Matrix	211	390	840	$13x10^{-6}$
Carbide	286	-	-	$6x10^{-6}$

RESULTS AND DISCUSSION

In the compression test, HAYNES 230 exhibits very typical composite behavior in the lattice-parameter strains during loading. The behavior is consistent with existing studies [10-12] and known composite FEM's [9]. As shown in Figure 3a, little lattice-parameter strain accumulates in the matrix after the macroscopic yield of 390 MPa. Furthermore, the matrix behavior matches that of the FEM model very well. To preserve the force balance, this implies that the carbides take up additional stress (elastic strain) in the lattice after macroscopic yield. The strain in the 333 carbide reflection in the transverse direction exhibited this trend which agreed well with the FEM results. It should be noted that there is a small, but significant difference between the experimental and predicted data in the matrix in the transverse direction. The calculated response of the matrix accumulates less elastic strain in the transverse direction than observed.

At this stage, the model, other than thermal stresses, contains nothing capable of producing tension-compression asymmetry. Thus, the calculated lattice response is necessarily similar in tension and compression. However, the measured lattice response

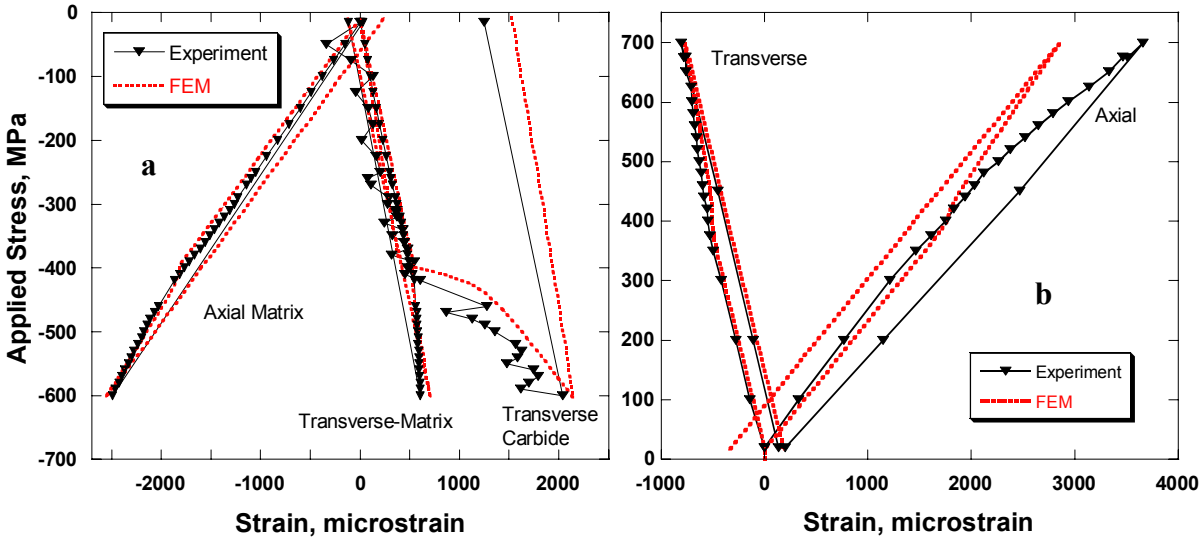

Figure 3: Experimental lattice parameter strains versus FEM strains in: (a) compression, and (b) tension.

to applied tension is strongly disparate from the response to compression (Figure 2b). While the thermal residual strains will cause a small disparity in the behavior of tension and compression in a typical composite, the difference shown in Figure 2b cannot be explained by residual strains alone. As shown in Figure 3b, in tension, the matrix accumulates elastic strain in the axial direction at an increasing rate following macroscopic yield at 390 MPa, while the model predicts (and the behavior in compression shows) that little elastic strain should evolve in the matrix after yield. In contrast, the transverse response of the matrix was very well captured by the model. Again the 333 carbide peak in the transverse direction is the only experimental carbide data available, but the statistics of this data are quite poor (200-500 με error bars). The general trend in the experimental carbide data agrees with the FEM prediction, but is omitted from the figure for clarity.

The tension-compression asymmetry is consistent with carbide debonding in tension which effectively prevents the expected load sharing between the carbide and the matrix in the axial direction. Perpendicular to the applied tensile load, Poisson's compression occurs, thus, no debonding takes place and the load transfer is as expected. The tensile behavior discussed here is consistent with previous *in situ* neutron results showing debonding in continuous fiber reinforced composites when loaded perpendicularly to the fiber direction [12]. Similarly, in compression, no debonding occurs parallel to the applied load. However, perpendicular to the applied compressive load, Poisson's tension occurs which may be too weak to lead to debonding, or may only cause small amounts of debonding. Weak debonding may be responsible for the subtle differences between the experimental and predicted behavior of the matrix in the transverse direction during the compression test (Figure 3a). Microscopy and more sophisticated FEM models, including debonding mechanisms, are ongoing to confirm the proposed mechanism.

CONCLUSIONS

The observed disparity between the measured and predicted lattice response to applied tension and compression in HAYNES 230 can be explained by debonding of the carbides in the loading direction during tensile loading, effectively preventing load transfer from occurring. In contrast, in compression, the load transfer between the carbides and the matrix is composite-like as expected. Microscopy and FEM work should be able to confirm if the behavior proposed here is realistic.

REFERENCES

1. HAYNES 230 Alloy Product Brochure, H-3000, Haynes International. www.haynesint.com
2. M. R. Daymond, M. A. M. Bourke, R. B. Von Dreele, B. Clausen and T. Lorentzen, *J. Appl. Phys.* **82**, 4, (1997).
3. M. A. M. Bourke, D.C. Dunand, and E. Ustundag, *Appl. Phys. A* **74**, S1707–S1709 (2002).
4. H. J. Stone, T. M. Holden, and C. R. Reed, *Acta Mater.* **47** (17), 4435-4448 (1999).
5. H. Choo, M. A. M. Bourke, P. Nash, M. Daymond, N. Shi, *Mat. Sci. & Eng, A.* **264**, 108-121 (1999).

6. ASTM Standard E 8-04, *Standard Test Methods for Tension Testing Metallic Materials* 6.
7. A.C. Larson and R.B. Von Dreele, *Los Alamos National Laboratory Report* LAUR 86-748 (2000).
8. ABAQUS User Manual, version 6.3, Hibbitt, Karlsson and Sorensen, Inc., (2002) www.abaqus.com.
9. B. Clausen, S.-Y. Lee, E. Üstündag, C.C. Aydiner, R.D. Conner, M.A.M. Bourke, *Scripta Materalia* **49** (2), 123-128, (2003).
10. A. J. Allen, M. A. M. Bourke, S. Dawes, M. T. Hutchings, P. J. Withers, *Acta Metallurgica et Materialia* **40** (9), 2361-73 (1992).
11. G. L. Povirk, M. G. Stout, M. Bourke, J. A. Goldstone, A. C. Lawson, M. Lovato, S. R. Macewen, S. R. Nutt, A. Needleman, *Acta Metallurgica et Materialia* **40** (9), 2391-412 (1992)
12. P. J. Withers, A. P. Clarke, *Acta Materialia* **46** (18), 6585-98 (1998).